WANG XIN[1*], LING JINLONG[1]

COMPARISON AND ANALYSIS ON THE EFFECTS OF OIL-QUENCHING AND SALT-QUENCHING FOR CARBURIZED GEAR RING

The most commonly quenching process for carburizing gears is the oil-quenching (OQ) and salt-quenching (SQ), and finite analysis and comparison of OQ and SQ on the carburizing gear ring were performed. Wherein, the accurate simulation of gear carburization was obtained by the alloying element coefficient for diffusion coefficient and experiment validation. The heat transfer coefficients measured by the inverse heat transfer method was used to the temperature simulation, and the gear distortion mechanism was analyzed by the simulated results. By the comparison of OQ, SQ had higher cooling capacity in the high temperature region and slow cooling rate in the temperature range where martensite transformation occurs. The martensite transformation was more sufficient, and the compressive stress of the tooth was greater in the SQ. The tooth showed a drum-shaped and slight saddle-shaped distortion in the OQ and SQ, respectively. The simulated distortion results have good consistency with the measured results, and the SQ distortion was more uniform and stable based on the measured results.

Keywords: oil-quenching; salt-quenching; martensite transformation; distortion

1. Introduction

Carburizing-quenching (CQ) has become the main surface treatment process of the heavy-duty gears manufacturing. The surface and core of the gear have temperature, microstructure, and stress changes, which cause the gear to be distorted. The distortion of CQ has become one of the prominent technical difficulties in gear manufacturing, and it is closely related to the quenching process and medium [1-2]. At present, the most common quenching medium for carburizing gears is the quenching oil and low temperature salt. Wherein, the production cost of the oil-quenching (OQ) is high, the distortion is large, and the quality is less stable. The salt-quenching (SQ) can significantly reduce the gear distortion, and it has high production efficiency and low maintenance costs, but note that the treatment of exhaust gas and the explosion danger. Many results that cannot be extracted by traditional experiment and experience can be obtained by the numerical simulation. It provides an effective way to reveal the law of distortion and control the distortion on carburizing gear, and it has become the frontier in the international heat treatment field [3].

Zhang et al. [4] compared the hardness of 17CrNiMo6 gear samples in the SQ and OQ, and found that the former has higher cooling capacity and core hardness. Based on the finite element analysis, Wang et al. [5] changed the oil into the low-temperature salt for quenching, the distortion of the large gear shaft was greatly reduced. Gu et al. [6] analyzed the effects of different SQ processes on the properties of carburizing steel 18Cr2Ni4W. Based on the results of the residual austenite and surface hardness, the three temperature parameters of austenitizing, salt bath and air cooling were optimized. The above conclusions were provided by the experimental results and theoretical analysis, and had not been quantitatively analyzed and calculated. There are few researches about the simulation comparison of both quenching processes on the carburizing gear. In this study, a carburizing locomotive gear was selected as the sample, the numerical simulation of the OQ and SQ proceeds by DEFORM. The simulated temperature, phase transformation and stress-strain results of both processes were analyzed and compared. Some experimental results were used to establish and verify the model.

2. Finite element and experiment analysis

2.1. Analysis model and material

The shape and dimension, and analysis experiment model of a locomotive gear ring, is depicted as shown in Fig. 1. In order to simplify analysis, a single tooth model is built using the

[1] HENAN UNIVERSITY OF ENGINEERING, MECHANICAL ENGINEERING COLLEGE, ZHENGZHOU, HENAN 451191 CHINA

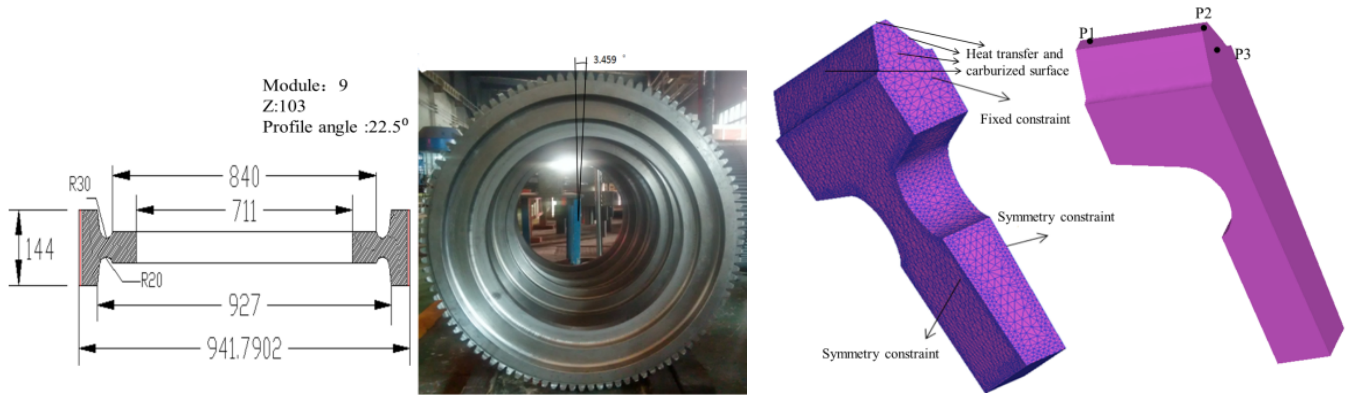* Corresponding author: haiyang630@163.com

Fig. 1. Gear structure and analysis model

symmetric as model 50000 tetrahedral elements. Considering that the gear is laid flat in the furnace, a fixed constraint is implemented on the end of the gear. For easy to extract the results, three tracking points were selected. That is, P1 was the surface point at the end of the gear, and P2 and P3 were the surface and core points in the middle of the tooth width. The measured diameter change was compared with the simualted results. The gear is made of 17CrNiMo6, and the chemical composition is shown in TABLE 1.

Fig. 2. Carburizing process using carbon potential (CP) 1.15 and 0.85

TABLE 1

The content of the main alloying elements.

Elements	C	Si	Mn	Cr	Mo	Ni
Wt.%	0.17	0.25	0.8	1.41	0.29	1.26

2.2. Key simulation parameters

The carburizing process proceeded in a 450 KW pit carburizing furnace, as shown in Fig. 2. The carbon diffusion calculation used Fick's law [7]. Wherein, the mass transfer coefficient was 0.0001123 mm/s when the temperature is 930°C [8]. As Kim [9] pointed out, the diffusion coefficient (D) was formulated by considering the effects of temperature and carbon content. In the present, the calculation of D adds the effect of the alloying elements, as follows:

$$D = \left(0.0047 \exp\left(-1.6C\right) \exp\left[\frac{-\left(37000 - 6600C\right)}{RT} \right] \right)$$
$$\left(\begin{array}{c} 0.013\%\text{Mn} + 0.013\%\text{Mo} + \\ + 0.040\%\text{Cr} - 0.055\%\text{Si} - 0.014\%\text{Ni} \end{array} \right) \quad (1)$$

Where, T and C denote the temperature (°C) and carbon content (wt.%), respectively, and each term denotes the mass percentage of the alloy element, as shown in TABLE 1. The equation is derived from a large amount of empirical data. The calculated D is shown in Fig. 3.

In the present study, quenching oil was KR218 with a temperature of 60°C, the constituent of the salt is 55% KNO$_3$,
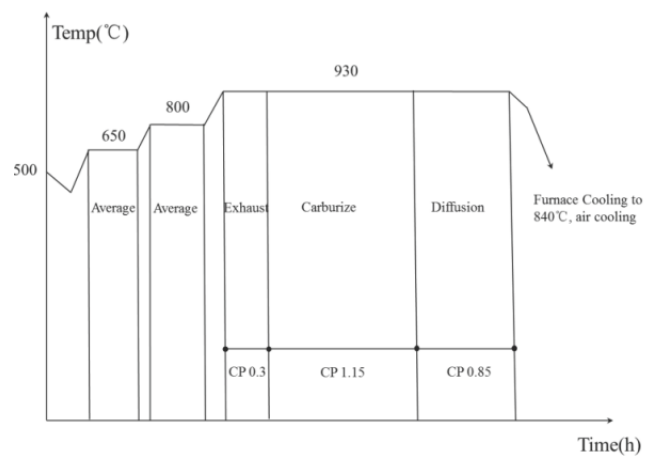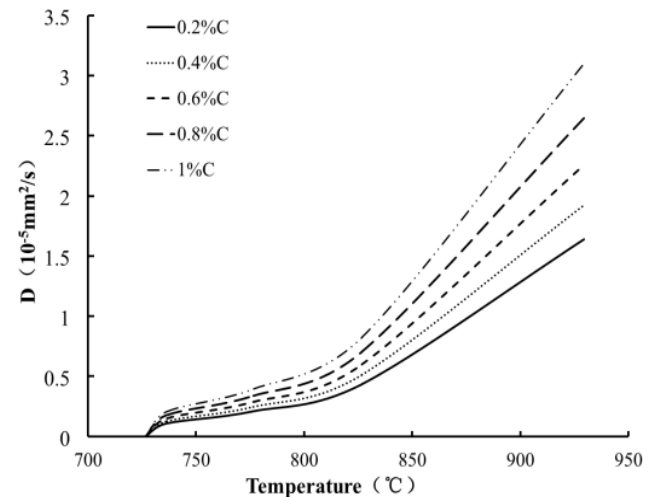

Fig. 3. D adding alloying element influence

45%NaNO$_2$ and 0.7 wt.% of water. The temperature of the salt was 160°C. The cooling curve of the quenching medium was measured by a cooling performance tester that meets the ISO 9950:1995(E) standard, as shown in Fig. 4. Based on the cooling curve, the inverse heat transfer method firstly discretizes the cooling curve, then calculates the heat flux density by the least square method, and finally obtains the heat transfer coefficient
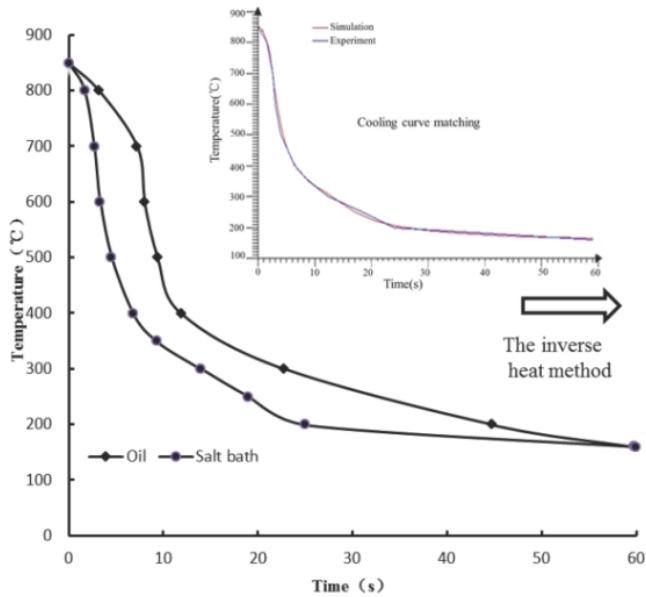
Fig. 4. HTC calculated by the inverse heat method

(HTC) by solving the thermal differential equation [10-11]. The simulated cooling curve was matched with the experiment curve by continuous verification, and the HTC was calculated by DEFORM, as shown in Fig. 4.

The maximum HTC of the salt and quenching oil are 22 W/(mm$^2 \cdot$ °C) and 5.6 W/(mm$^2 \cdot$ °C) respectively, which correspond to temperatures 560°C and 450°C, respectively. In the high temperature range higher than 470°C, the HTC of the salt is greater than that of the oil, while in the low temperature range, the HTC of both media is similar. The temperature of the salt bath is higher than that of the oil, so the cooling rate of the salt is lower than that of the oil in the low temperature range. It shows that the salt has stronger cooling capacity in the high temperature range, which reduces the possibility of non-martensite transformation. In the low temperature range, the salt has the characteristics of slow cooling rate, which makes the martensite finer and the transformation stress smaller.

The martensite transformation considering the temperature and carbon content was calculated the modified Magee's equation. Wherein, the martensite transformation start temperature (M_s) was calculated based on the following equation with carbon content [12-14].

$$M_s = 548 - 440C - \left(\begin{array}{c} 14Si + 26Mn + 11Cr + \\ + 14Ni + 9Mo \end{array} \right) \quad (2)$$

The total strain is assumed to be divided into elastic, plastic, thermal, phase transformation, transformation induced plasticity strains [12]. During quenching, the phase transformation strain mainly depends on the volume expansion of the martensite, and the thermal strain is induced from the cooling shrinkage. Both strains counterbalance each other and eventually cause gear distortion. While the thermal and phase transformation strains have a significant impact on the distortion.
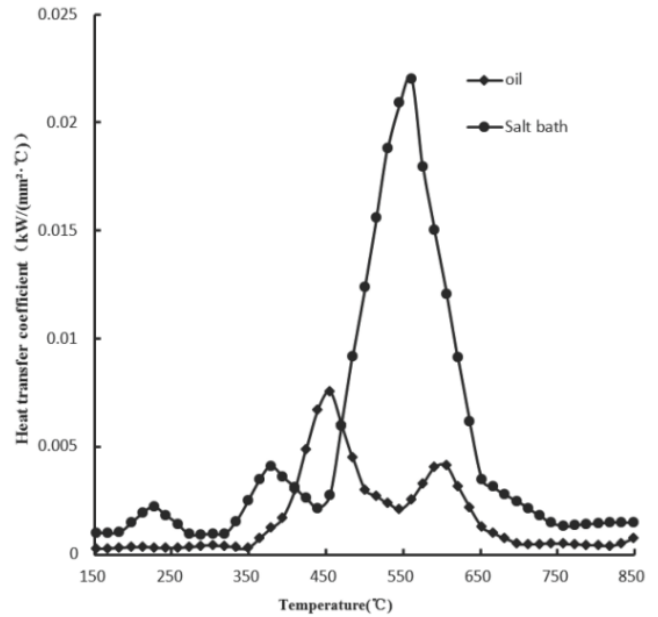
3. Results analysis and comparsion

3.1. Carburizing results

The surface carbon content of the furnace sample was determined to be 0.79% by the X-350A spectrometer after carburization. Fig. 5 shows the carbon distribution in the middle of the tooth width, and the maximum carbon content is 0.8%. Both results are basically consistent. Due to the convex and concave structure, the carbon content near the addendum is obviously higher than that of the other position on the curve. According to the standard of the gear carburizing case, starting from the surface, the depth of carbon content greater than 0.35% is the carburized case. So the carburizing case at the three positions was about 3-4 mm.
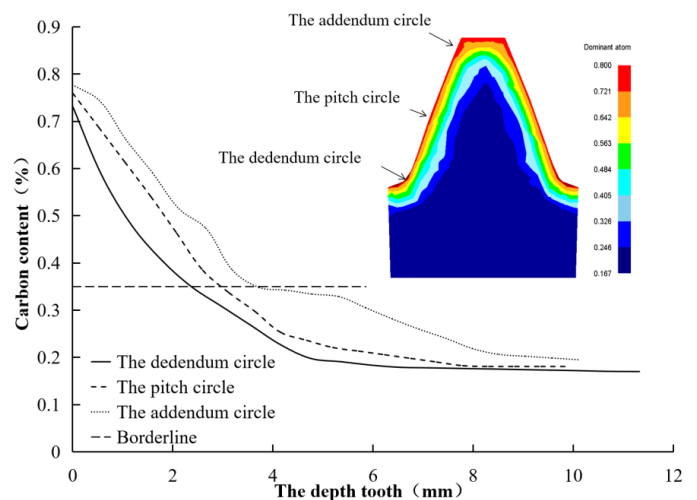

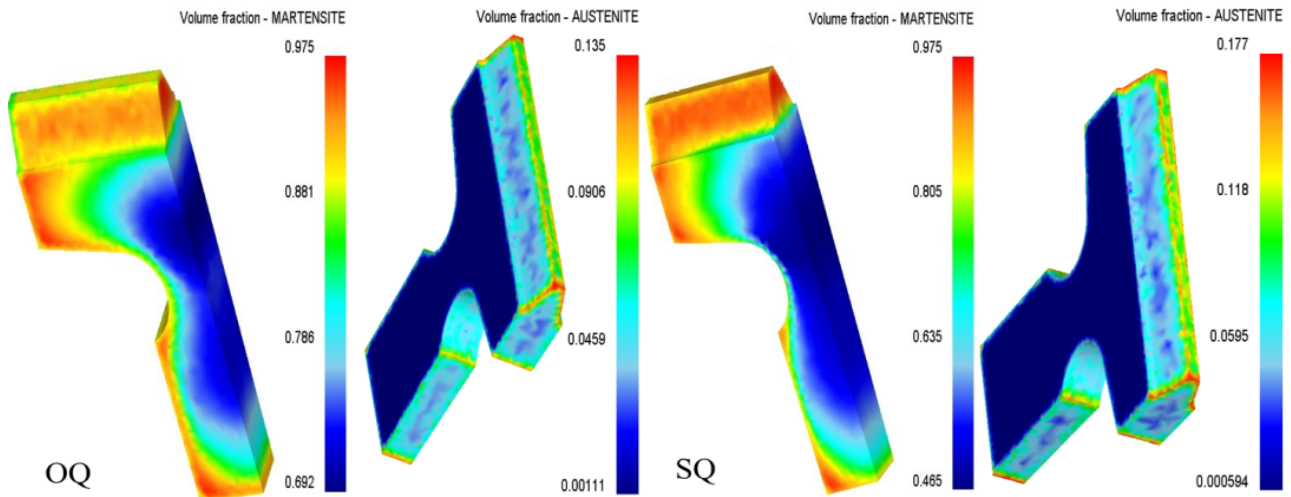Fig. 5. Distribution results of carbon content on the addendumcircle, pitch circle and dedendum circle

1270

Fig. 6. Martensite and residual austenite results of OQ and SQ

3.2. Phase transformation results

After salt-cooling and oil-cooling, the gears were air-cooled to room temperature. Fig. 6 shows the volume fraction of martensite and residual austenite results in the OQ and SQ. Most tooth was transformed into martensite in both processes, and the maximum martensite content is 97.5%, which is distributed in the core of the tooth. A small amount of austenite remained on the tooth surface. The maximum austenite content in the SQ is 17.7%, which is slightly more than that in the OQ. In the SQ the martensite transformation on the surface proceeded in air, and the air-cooling rate is slower, which increased the stability of austenite, so more austenite remained. More residual austenite reduces the volume expansion during quenching, which is conducive to the reduction of gear distortion. The volume fraction of austenite and martensite after salt-cooling, and before air-cooling in the SQ were shown in Fig. 7. A large amount of austenite remained on the surface of the tooth, and the highest valve was 98.2%. The carbon content of the tooth surface is 0.8%. The Ms at this position is 152℃, which is lower than the temperature of the salt. So the martensite transformation had not occurred on the surface. Nearly half of the carburizing case has not yet completed the martensite transformation based on
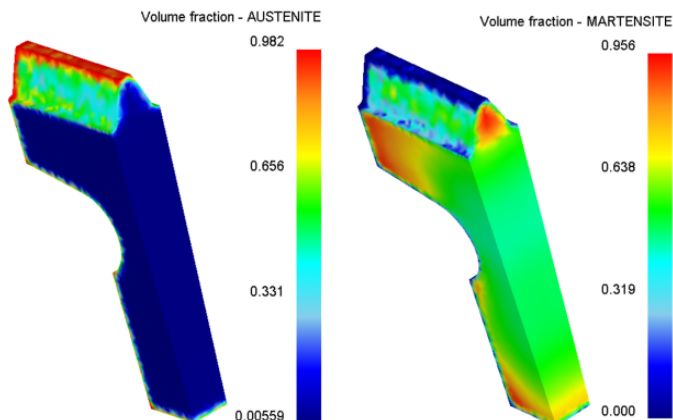
Eq. 2. The core area of the tooth had completed the martensite transformation, and the maximum martensite content is 95.6%. Hence, the martensite transformation occurs in different step in the SQ. Firstly, the core with the low carbon content occurs and completes the martensite transformation during the salt-cooling process, and then the martensite transformation is completed on the surface with high carbon content during air-cooling. Due to the low oil temperature, the martensite on the surface and the core was completed in the OQ. Fig. 8 shows the surface and core microstructure in both processes. The surface microstructure in both processes are needle martensite, residual austenite and free ferrite, but the austenite content is higher in the SQ. The core microstructure in both processes contains lath martensite, but the SQ martensite is relatively finer. It is mainly due to the slow cooling rate in the temperature range of martensite transformation, it make small volume expansion and stress.
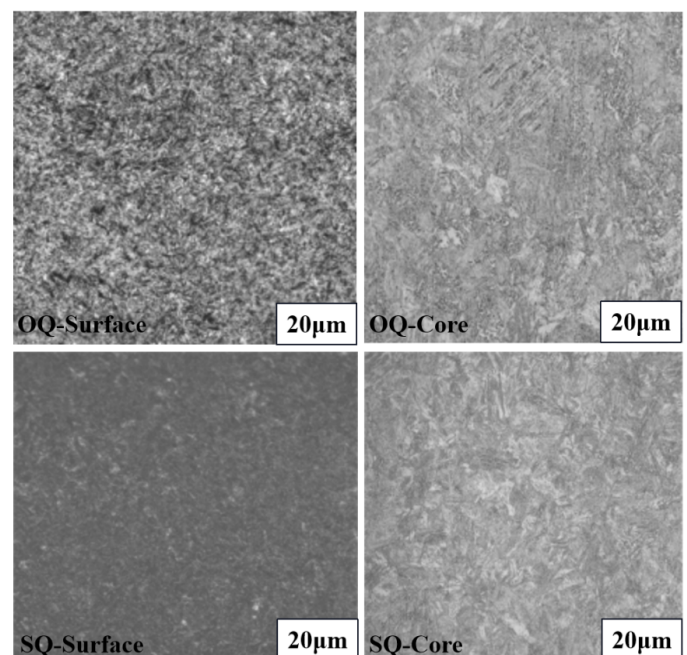

Fig. 7. Austenite and martensite content before air cooling

Fig. 8. Surface and core microstructure of OQ and SQ

3.3. Stress and distortion results

Fig. 9 shows the axial stress along the depth at the addendum in the middle of the tooth width in both processes. Due to different temperature and phase transformation change, the axial stress was compressive stress in the surface, and gradually became tensile stress in the core. The maximum compressive stresses in both processes were 78 MPa and 114 MPa, respectively, and their positions were 3.5 mm and 3.8 mm from the surface, respectively. The compressive stress of the SQ is significantly higher than that of the OQ. In the OQ, the martensite transformation in the surface and core is completed in one step, while the surface and core martensite transformation in the SQ is occurred in two steps. The martensite graded transformation is more sufficient and obtainable in the SQ. It is guaranteed that the gear can obtain a relatively large compressive stress.

Fig. 10 shows the radial displacement of the three points in the OQ. The displacement trend of three points is basically the same. In the first 52s, due to less martensite was produced, the volume expansion caused by the martensite transformation was small, the displacement was mainly manifested as the volume contraction caused by the oil-cooling. Therefore, the radial displacement of three points decreased rapidly. Compared with the other points, point P1 had a faster cooling rate, so its displacement decreased the most. Then when the time is 142s, the martensite transformation of the three points is basically completed. The radial displacement caused by the martensite transformation is more than that caused by the cooling, the radial displacement of three points shows a slight expansion. The martensite transformation at point P3 occurred first, so its radial displacement is the maximum. The carbon content of the other points were high, and the martensite transformation occurred late, the volume expansion caused by the martensite transformation was hindered by the high-strength martensite of the core, and its cooling rate was relatively high, so the final radial expansion was smaller than that of point P3. Point P1 had a faster cooling rate and more cooling shrinkage than point P2, so the volume expansion of point P1 is less than that of point P2. The cooling rate of point P1 was faster than the other two points, and the cooling shrinkage was the most. Therefore, the displacement of point P1 was much smaller than that of the other two points. When the martensite transformation was completed, the temperature will continue to decrease slowly, and the martensite thermal expansion is much smaller than that of other phases. So the radial displacement of the three points still appearred to decrease slowly, but the final displacement also manifested as radial expansion.

In summary, due to different phase transformation and temperature change, both processes had different distortion. Fig. 11 shows the radial distortion of the gear in the OQ and SQ. Except for a slight contraction near the two ends, the whole width presents the expansion along the tooth width in the OQ. Due to the fast cooling, the end shows slight shrinkage. The tooth presents a drum-shaped distortion along the tooth width. The middle of the tooth width expands mostly. The maximum is 0.325 mm, so

the diameter expands by 0.65 mm. Along the drum-shaped curve, the maximum expansion difference is 0.3 mm. It corresponds to the displacement difference between P1 and P2 in Fig. 10. The middle distortion is larger than the end distortion mainly due to the more martensite and less residual austenite content at the end (Fig. 6), which causes more volume expansion and less cooling shrinkage. In the SQ, the radial distortion is still expansion, The gear tooth showed a slight saddle-shaped distortion along the width. Near the middle of the width, the diameter expansion was 0.3 mm, the expansion was 0.414 mm near the end, and the difference was only 0.114 mm, which was more uniform than that in the OQ. Based on the phase transformation results, the martensite transformation occurs in different step in the SQ. More residual austenite reduces the volume expansion, and surface martensite transformation is completed in air-cooling with the slow cooling rate, so the SQ distortion is smaller than the OQ distortion. And due to the large cooling capacity of the salt in the high temperature range, the core martensite content in the middle of the width is slightly higher, which hinders the expansion of the surface martensite, so the middle distortion is slightly smaller than the end distortion.
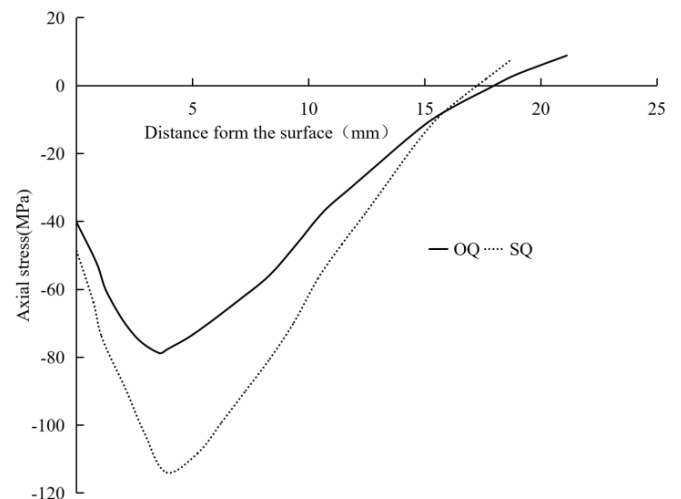

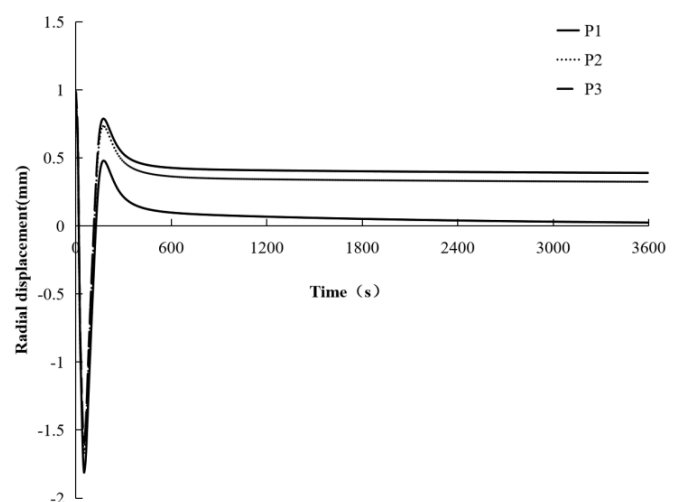
Fig. 9. Axial stress along the surface depth

Fig. 10. The radial displacement evolution of the three points in the OQ

1272

The 10 OQ gears and 6 SQ gears were selected with the furnace. The average radial displacement of these gears in the middle of the tooth width were measured, as shown in Fig. 11. The range of OQ distortion is 0.18-0.92 mm, the distortion values are relatively unstable. The average value is 0.532 mm, which is slightly smaller than the simulated maximum value, but the difference is only 0.12 mm. It indicates that the simulation accuracy may be guaranteed. The range of SQ distortion is 0.3-0.5 mm, which is in good agreement with the results. It is obvious that variation the SQ distortion is more stable than the OQ distortion. So if the environment and explosion hazard are not considered, the SQ process is more conducive to improving the gear distortion.

4. Conclusions

(1) By considering the alloying element coefficient and experiment verification, the accurate simulation of gear carburization has been achieved. The heat transfer coefficients were obtained by the inverse heat transfer method, and the temperature and phase transformation simulations were realized. The gear distortion was simulated and its mechanism was analyzed. The simulated distortion have good consistency with the measured results.

(2) In the OQ and SQ, the simulation shows that the martensite transformation starts from the core, and then occurs in higher-carbon area on the tooth surface. But the martensite transformation in the SQ is more sufficient, so that it can obtain a larger surface compressive stress.

(3) In the OQ, the simulation depicts that the tooth showed a drum-shaped distortion, and the maximum diameter expansion was 0.65 mm. In the SQ, except for both ends, the tooth showed a slight saddle-shaped distortion. The maximum expansion was 0.414 mm, and the SQ distortion was relatively uniform and stable.

Fig. 11. Radial deformation results of OQ (a) and SQ (b); Experiment distortion results (c)

REFERENCES

[1] J.G. Chen, Research of Distortion Control for Carburized Quenching Gear, Journal of Mechanical Transmisssion **38** (5), 152-156 (2014).
DOI: https://doi.org/10.16578/j.issn.1004.2539. 2014.05.002

[2] S. Raygan, J. Rassizadehghani, M. Askari, Comparison of Microstructure and Surface Properties of AISI 1045 Steel After Quenching in Hot Alkaline Salt Bath and Oil, Journal of Materials Engineering & Performance **18** (2), 168-173 (2009).
DOI: https://doi.org/10.1007/s11665-008-9273-x

[3] T. Sugimoto, M. Qin, Y. Watanabe, Computational Study of Gas Quenching on Carburizing Hypoid Ring Gear, B. H. M. **151**, 451-461 (2006). DOI: https://doi.org/10.1007/BF03165207

[4] L. Zhang, A.X. Wang, M. Gu, B.K. Li, Q.L. Zhu, Martempering In Molten Nitrate and Oil Quenching Processes of 17CrNiMo6 Steel Carburized Gear, Heat Treatment of Metals **41** (2), 146-149 (2016). DOI: https://doi.org/10.13251/j.issn.0254-6051. 2016.02.034
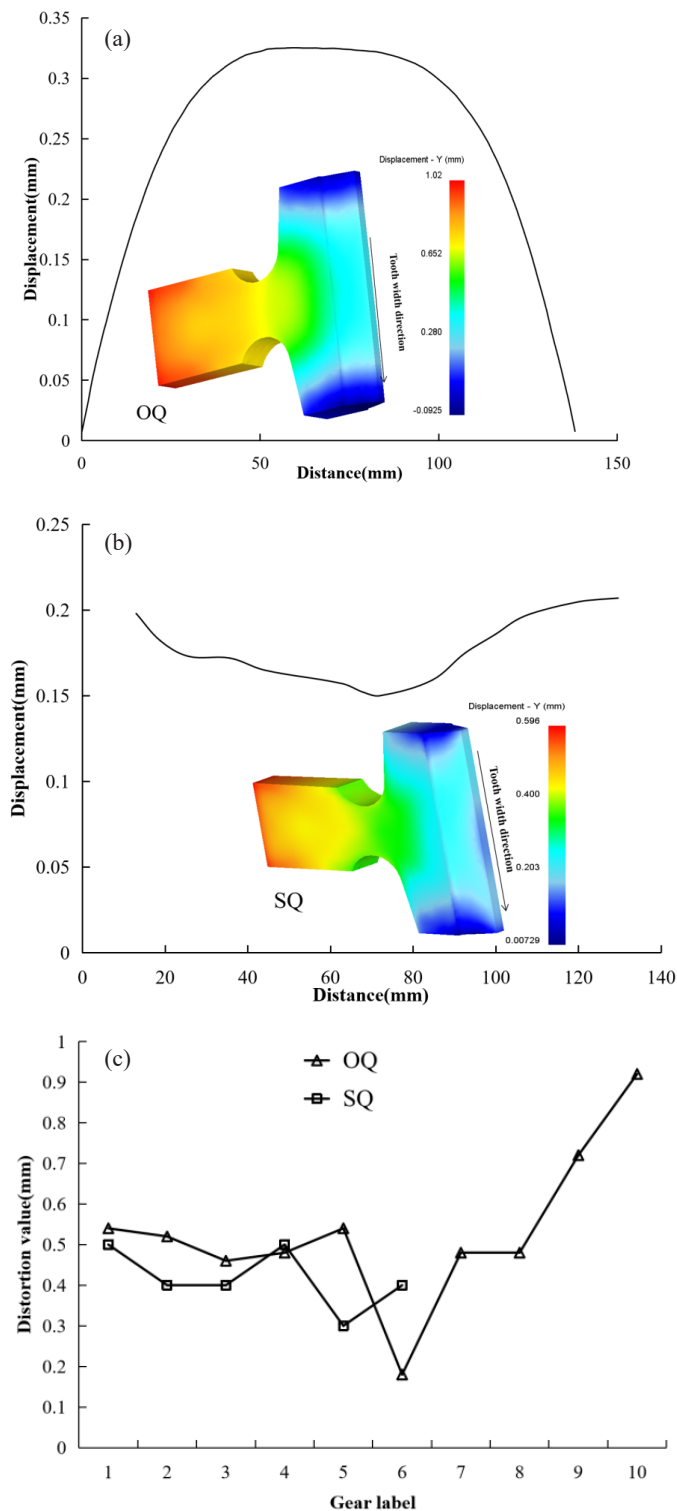
[5] X. Wang, B.K. Li, M. Gu, S.X. Li, Distortion Control of Large Carburized Gear Shaft Based on Finite Element Analysis, Heat Treatment of Metals **44** (4), 239-242 (2019).
DOI: https://doi.org/10.13251/j.issn.0254-6051. 2019.04.048

[6] X.M. Gu, L.B. Lü, J.W. Liu, Effect of Salt Bath Quenching After Carburizing on Microstructure and Property of 18Cr2Ni4W Steel, Heat Treatment of Metals **42** (5), 184-188 (2017).
DOI: https://doi.org/10.13251/j.issn.0254-6051. 2017.05.038

[7] N.K. Kim, K.Y. Bae, Analysis of Deformation in the Carburizing-quenching Heat Treatment of Helical Gears Made of SCM415H Steel, International Journal of Precision Engineering and Manufacturing **16** (1), 73-79 (2015).
DOI: https://doi.org/10.1007/s12541-015-0009-1

[8] X. Zhang, J.Y. Tang, Key Technology in Carburizing Process Simulation for 17CrNiMo6 Steel Annular Gear, Heat Treatment of Metals **40** (3), 185-189 (2015).
DOI: https://doi.org/10.13251/j.issn.0254-6051. 2015.03.042

[9] D.W. Kim, Y.G. Cho, H.H. Cho, S.H. Kim, W.B. Lee, M.G. Lee, H.N. Han, A Numerical Model for Vacuum Carburization of An Automotive Gear Ring, Metals & Materials International **17** (6), 885-890 (2011).
DOI: https://doi.org/10.1007/s12540-011-6004-x

[10] A. Sugianto, M. Narazaki, M. Kogawara, Distortion Analysis of Axial Contraction of Carburized-quenched Helical Gear, Journal of Materials Engineering and Performance **19** (2), 194-206 (2010).
DOI: https://doi.org/10.1007/s11665-009-9476-9

[11] X. Wang, B.K. Li, M. Gu, Simulation Analysis on Martempering in Salt Bath Technology for Carburized Distortion Sample, Metallurgical & Materials Transactions A **50** (2), 3758-3766 (2019).
DOI: https://doi.org/10.1007/s11661-019-05277-y

[12] A. Sugianto, M. Narazaki, M. Kogawara, A. Shirayori, S.Y. Kim, S. Kubota, Numerical Simulation and Experimental Verification of Carburizing-quenching Process of SCr420H Steel Helical Gear, Journal of Materials Processing Tech. **209** (7), 3597-3609 (2009).
DOI: https://doi.org/10.1016/j.jmatprotec.2008.08.017

[13] Y. Liu, S.W. Qin, Q.G. Hao, N.L. Chen, X.W. Zuo, Y.H. Rong, Finite Element Simulation and Experimental Verification of Internal Stress of Quenched AISI 4140 Cylinders, Metallurgical & Materials Transactions A **48** (3), 1402-1413 (2017).
DOI: https://doi.org/10.1007/s11661-016-3916-6

[14] X. Zhang, J.Y. Tang, X.R. Zhang, An Optimized Hardness Model for Carburizing-quenching of Low Carbon Alloy Steel, J. Cent. South Univ. **24** (1), 9-16 (2017).
DOI: https://doi.org/10.1007/s11771-017-3403-2